Biochimica et Biophysica Acta 1787 (2009) 221–233

Contents lists available at ScienceDirect

Biochimica et Biophysica Acta

journal homepage: www.elsevier.com/locate/bbabio

The chemistry of the Cu_B site in cytochrome *c* oxidase and the importance of its unique His–Tyr bond

Ville R.I. Kaila [a,*], Mikael P. Johansson [b], Dage Sundholm [c], Liisa Laakkonen [d], Mårten Wikström [a,*]

[a] Helsinki Bioenergetics Group, Programme of Structural Biology and Biophysics, Institute of Biotechnology, University of Helsinki, P.O. Box 65, FI-00014 Helsinki, Finland
[b] Lundbeck Center for Theoretical Chemistry, Aarhus University, DK-8000 Århus C, Denmark
[c] Department of Chemistry, University of Helsinki, P.O. Box 55, FI-00014 Helsinki, Finland
[d] Division of Biochemistry, Department of Biological and Environmental Sciences, Faculty of Biosciences, University of Helsinki, FIN-00014, Helsinki, Finland

ARTICLE INFO

Article history:
Received 13 August 2008
Received in revised form 7 January 2009
Accepted 9 January 2009
Available online 20 January 2009

Keywords:
Oxygen reduction
Proton transfer
DFT
Quantum chemistry

ABSTRACT

The Cu_B metal center is at the core of the active site of the heme–copper oxidases, comprising a copper atom ligating three histidine residues one of which is covalently bonded to a tyrosine residue. Using quantum chemical methodology, we have studied the Cu_B site in several redox and ligand states proposed to be intermediates of the catalytic cycle. The importance of the His–Tyr crosslink was investigated by comparing energetics, charge, and spin distributions between systems with and without the crosslink. The His–Tyr bond was shown to decrease the proton affinity and increase the electron affinity of both Tyr-244 and the copper. A previously unnoticed internal electronic equilibrium between the copper atom and the tyrosine was observed, which seems to be coupled to the unique structure of the system. In certain states the copper and Tyr-244 compete for the unpaired electron, the localization of which is determined by the oxygenous ligand of the copper. This electronic equilibrium was found to be sensitive to the presence of a positive charge 10 Å away from the center, simulating the effect of Lys-319 in the K-pathway of proton transfer. The combined results provide an explanation for why the heme–copper oxidases need two pathways of proton uptake, and why the K-pathway is active only in the second half of the reaction cycle.

1. Introduction

Cytochrome *c* oxidase (CcO) is the terminal enzyme in the respiratory chain of mitochondria and several bacteria. By reducing molecular oxygen to water CcO drives the respiratory chain and contributes to the generation of an electrochemical proton gradient across the membrane, which is used for example to drive the synthesis of ATP by F_oF_1-ATPase [1–3]. High resolution X-ray structures of CcO have been available for over ten years [4,5], and details of the mechanism of proton pumping and oxygen reduction have been studied in a multitude of both experimental [6–10] and theoretical works [11–16]. Although many mechanistic principles are already understood, some crucial questions still remain; *e.g.* why are two pathways required for proton uptake from the negatively charged N-side of the membrane (Fig. 1)?

Electrons are fed stepwise to CcO from the soluble cytochrome *c* (cyt *c*). The electrons are first accepted by the dinuclear Cu_A site (Fig. 1), which passes them further to a six-coordinated low-spin heme *a* center in a process that is followed by loading of a pump site with a proton taken up from the proton-conducting D-channel [9,10] (see Fig. 1). A conserved glutamic acid, Glu-242[1] at the end of the D-channel [17–20], has recently been suggested to work as a valve in minimizing leakage of the pumped proton back to the D-channel [21,22]. Protonation of the pump site raises the mid-point potential of the binuclear site, heme a_3/Cu_B, which accepts the electron from heme *a* together with a second proton from Glu-242 [23]. Uptake of the latter proton produces the equivalent of water at the binuclear site and repels the proton at the pump site, which is ejected to the P-side of the membrane [23,24].

The reduction of molecular oxygen to water takes place at the binuclear site, the active site of CcO, which is composed of a high-spin heme, heme a_3, and a copper center, Cu_B, which has three histidine ligands (His-240, His-290, and His-291, see Fig. 1). A tyrosine residue

Abbreviations: pmf, proton motive force; DFT, density functional theory; $E_{m,7}$, mid-point redox potential at pH 7 relative to NHE; CcO, cytochrome *c* oxidase; cyt *c*, cytochrome *c*; RMSD, root mean square deviation; *wt*, the model system of the "wild type" structure of the Cu_B site; His–Tyr "mutant", the *in silico* mutated model system of the Cu_B site, where the His–Tyr bond has been cut; MD, molecular dynamics; His, H — histidine; Tyr, Y — tyrosine; Lys, K — lysine; Y–OH, protonated Tyr; Y–O*, neutral Tyr-radical; Y–O$^-$, anionic Tyr (tyrosinate); PA, proton affinity; EA, electron affinity; HOMO, highest occupied molecular orbital; LUMO, lowest unoccupied molecular orbital

* Corresponding authors.
E-mail addresses: ville.kaila@helsinki.fi (V.R.I. Kaila), marten.wikstrom@helsinki.fi (M. Wikström).

[1] All amino acid numbers refer to the amino acid sequence of *Bos taurus* subunit I.

0005-2728/$ – see front matter © 2009 Elsevier B.V. All rights reserved.
doi:10.1016/j.bbabio.2009.01.002

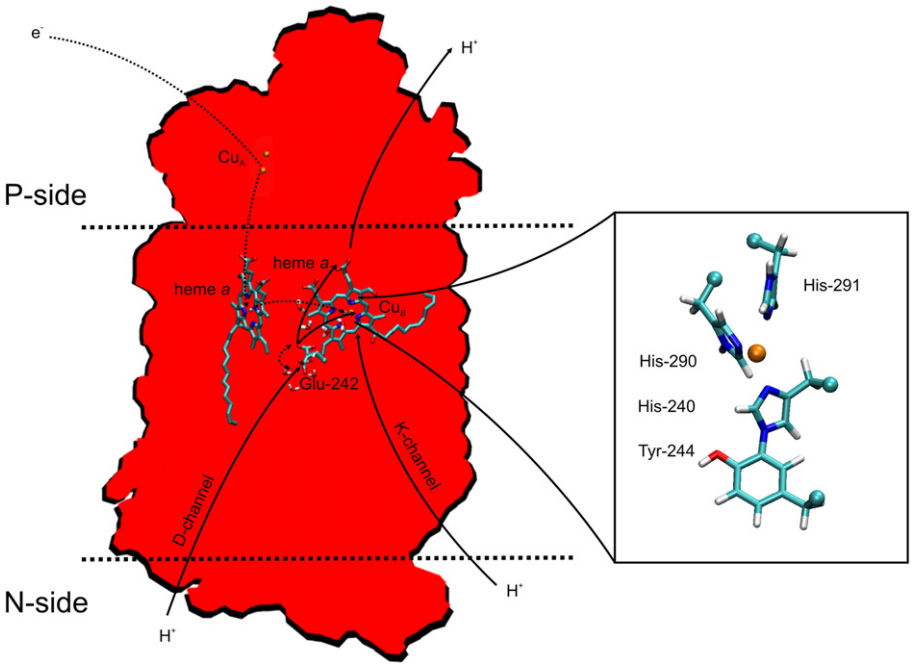

Fig. 1. The structure and location of redox groups in CcO. The electrons are transferred from cytochrome *c* (not shown) via Cu_A and heme *a* to the binuclear heme a_3/Cu_B site (dashed line). Protons are conducted via two proton conducting channels; the D-channel, ending up at Glu-242, and the K-channel ending up at Tyr-244. The protons are conducted from Glu-242 either to: 1) the pump site and further to the P-side of the membrane, or 2) to the binuclear heme a_3/Cu_B site. Inset: the structure of the Cu_B site.

(Tyr-244) is post-translationally crosslinked to one of the histidines (His-240), as shown by protein chemical and structural studies [4,25,26]. During the catalytic cycle of CcO the binuclear center cycles through different redox and ligand states. The redox cycle can be divided in an oxidative and a reductive phase (Fig. 2, Table 1). The oxidative phase starts by irreversible cleavage of the O–O bond, transferring four electrons and a proton to the oxygen molecule. Two electrons are taken from heme a_3, one from the copper, and one electron together with a proton are thought to derive from Tyr-244 [27]. This yields a species with ferryl iron, Fe[IV]=O, cupric copper and a neutral tyrosine radical, a state which for historical reasons is known as $\mathbf{P_M}$. However, the fourth electron in the oxygen cleavage reaction has recently been suggested to originate from a conserved tryptophan (Trp-126) producing a tryptophan radical that was suggested to relax in the $\mathbf{P_M}$ state [28,29]. In the next step of the cycle, $\mathbf{P_M}$ is reduced by an electron from heme *a*, yielding the $\mathbf{P_R}$ state. Due to the magnetic coupling between Cu_B and heme a_3, the Cu_B site is usually spectroscopically invisible. In $\mathbf{P_R}$, however, Cu_B shows a unique cupric EPR signal with a peak at $g \sim 2.24$ [30] and unchanged optical properties of the ferryl heme, relative to $\mathbf{P_M}$. It may therefore be concluded that the electron has been transferred to the tyrosine radical, producing a tyrosinate. Recent infrared studies have directly supported this conclusion [31]. Protonation of $\mathbf{P_R}$ yields the **F** state, in which the hydroxide ligand of Cu_B, which points towards the distal axial oxygen of heme a_3, is presumably protonated to water since the visible spectrum of the ferryl heme is strongly perturbed. Cu_B is EPR-silent [30] in this state, and the infrared feature of the tyrosinate is unchanged [31].

The protons consumed in oxygen reduction to water ("chemical" protons) are transferred to the binuclear site by two proton-conducting pathways, the D- and K-channels (named after Asp-91 and Lys-319, respectively). In the oxidative phase, the D-channel is used for conducting the chemical protons while in the reductive phase, starting at $\mathbf{O_H}$, the K-channel is employed for this purpose [32,33]. Whereas this holds for the members of the aa_3-type heme–copper oxidases, recent experiments have indicated that members of the ba_3-type family may employ only one proton conducting channel, and pump protons with only half of the proton-pumping stoichiometry of the aa_3-type oxidases [34–36].

The K-channel ends at residue Tyr-244. Reduction of $\mathbf{O_H}$ yields the $\mathbf{E_H}$ state, in which the charge transfer band of heme a_3 at 660 nm is shifted [9], a signal which has been suggested to be due to the interaction between ferric iron and cupric copper [37].

The Cu_B center is unique for the heme–copper oxidases and is different from other commonly found copper sites, *e.g.* type I–III copper centers [38,39], although the type II copper centers found in, *e.g.,* galactose oxidase, dopamine β-monooxygenase, and laccase, also have three histidine ligands [38,39]. The importance of the interesting His–Tyr crosslink in the Cu_B center has raised much discussion, and it has been suggested to lower the proton affinity of the tyrosine [26,40]. Studies on organic model compounds, such as 2-imidazol-1-yl-4-methylphenol, revealed that the covalent bond between the imidazol and phenol rings down-shifts the pK_a of the phenolic proton by 1.6 pK-units to 8.6, and increases the redox potential of the radical form by 66 mV to ~750 mV ($E_{m,7}$) [41]. In a recent quantum chemical study on a phenol–imidazol model system, the bond between the two aromatic moieties was also found to contribute to the proton and electron affinities; however, a copper atom, simulated as a point charge, was suggested to strongly contribute to the thermodynamic properties of the phenol [42]. Based on DFT studies, Daskalakis et al. recently suggested, that the importance of the His–Tyr crosslink is to fix the Cu_B center to a certain configuration in relation to heme a_3 [43]. However, this study focused on the CO-bound state of the Cu_B center and its IR-vibrations, without considering structural constrains from the protein backbone.

The effects of the different functionalities of the Cu_B center are difficult to decipher experimentally because amino acid substitutions at the center render the enzyme inactive. Here, we have therefore approached this problem by quantum-chemical methods employing a large (~110 atoms) realistic model of the Cu_B center that includes the crosslinked tyrosine. In the spirit of biological experiments, we call the original model with the His–Tyr crosslink a "wild type" system, whereas the model where the His–Tyr bond has been cut will be called a "mutation". The results conform well with some of the known

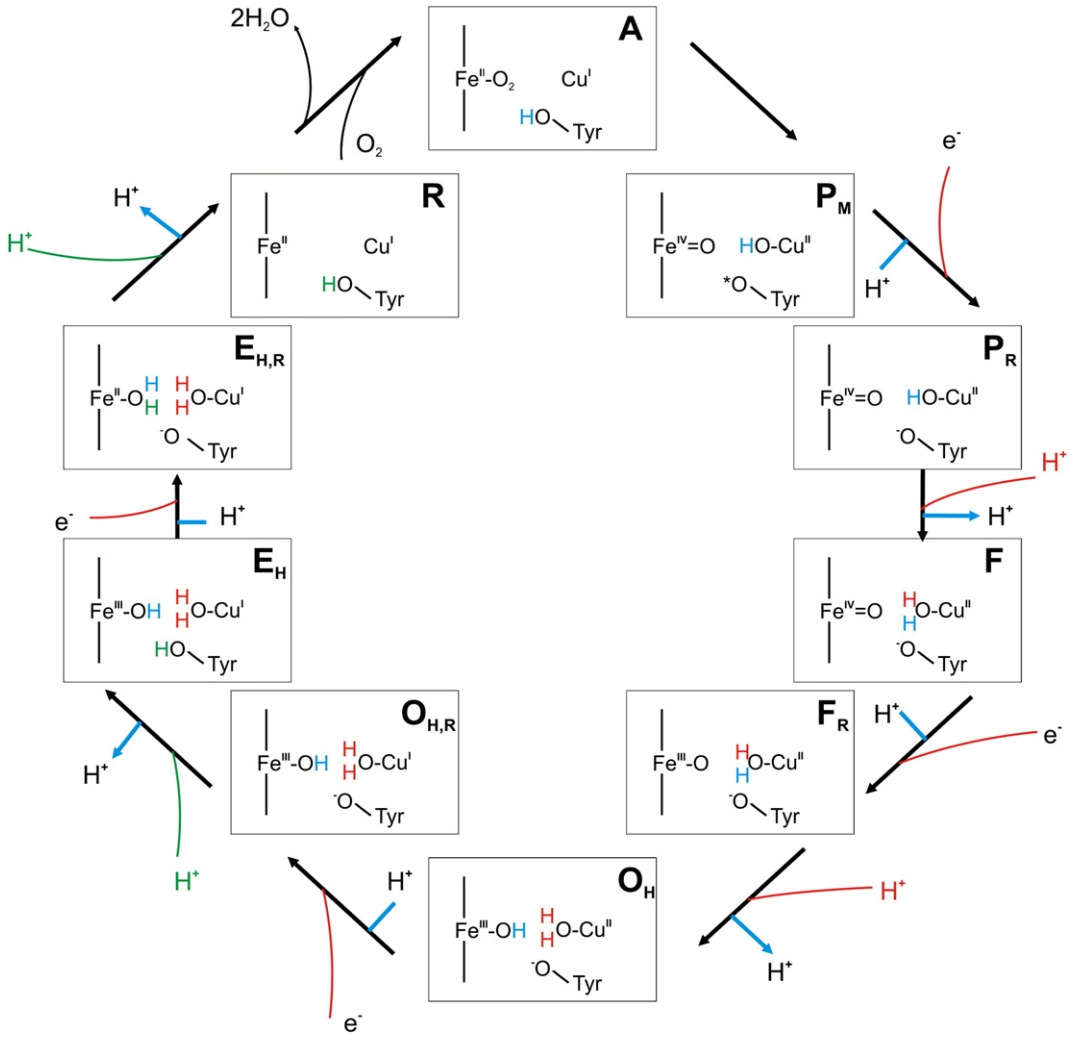

Fig. 2. Proposed reaction cycle of CcO. The cycle starts by cleavage of the O–O bond in the **A**→$\mathbf{P}_M$ transition. In each proton pumping step (**P**→**F**, **F**→**O**, $\mathbf{O}_H$→$\mathbf{E}_H$, and $\mathbf{E}_H$→**R**) one proton is transferred from Glu-242 to the proton loading site (blue arrow, H^+), an electron is transferred to the binuclear site (red arrow, e^-), a second proton is transferred to the binuclear site (red arrow, red or green H^+), and the proton is released from the proton loading site to the P-side of the membrane. The chemical protons are taken from D-channel in the oxidative phase (**P**→$\mathbf{O}_H$, red H^+), and from the K-channel in the reductive phase ($\mathbf{O}_H$→**R**, green H^+).

properties of this site, and bring forward new features that might elucidate the importance of the His–Tyr crosslink and the role of the K-channel in proton transfer.

2. Models and methods

Density functional theory (DFT) [44,45] has proven very suitable for the study of biological metal centers [46–53]. We have used the B3LYP hybrid functional [54,55] as the main methodology in this study, due to its established good performance. Benchmark calculations suggest that the B3LYP functional generally reproduces geometries with an accuracy of 0.04–0.05 Å and energetics with a mean error on the order of 3 kcal/mol [56]. For transition metal complexes, B3LYP calculations have yielded a somewhat larger error [57–62]. The Cu_B model was built from the structure of cytochrome *c* oxidase from *Bos taurus*, PDB entry 1V54 [63]. The effect of heme a_3 on Cu_B was tested in our previous study concerning the derivation of point charges for the metal centers in CcO, and was found to have only a minor contribution on the charge distribution of the Cu_B system [64]. Therefore, the heme was not included in the current calculations. It should also be pointed out that the effect of heme a_3 is expected to be the same on the "wild type" enzyme (wt) as on a variant system where the His–Tyr crosslink was abolished (see below), with the exception of the interaction to the farnesyl group of heme a_3. The structures of the Cu_B center in different ligand and redox states were optimized using a split-valence basis set augmented with polarization functions [65], on all atoms except copper, for which a triple-zeta valence basis set augmented with polarization functions [66] was used. The complete backbone of each amino acid was included in the model. In addition, each amino acid was capped with N-terminal methyl groups and C-terminal acetyl groups to simulate the continuation of the peptide chain. The effect of the protein surroundings was modeled by using the electrostatic continuum model COSMO [67] with a dielectric constant ε=4. Furthermore, the restraints imposed by the protein backbone were incorporated into the models

Table 1
Proposed intermediates of the catalytic cycle and their possible structures

State	Structure of BNC		$Q_{tot}(Cu_B)$	$S_{tot}(Cu_B)$
	heme a_3	Cu_B		
A	Fe[II]	Cu[I] YOH	+1 0	
$\mathbf{P}_M$	Fe[IV]=O	Cu[II]–OH YO*	+1	1
$\mathbf{P}_R$	Fe[IV]=O	Cu[II]–OH Y–O^-	0	1/2
F	Fe[IV]=O	Cu[II]–H_2O Y–O^-	+1	1/2
$\mathbf{O}_H$	Fe[III]–OH	Cu[II]–H_2O Y–O^-	+1	1/2
$\mathbf{E}_H$	Fe[III]–OH	Cu[I]–H_2O Y–O^-	0	0
R	Fe[II]	Cu[I] YOH	+1	0

Table 2
Geometrical properties of the "wild type" (first number) and the "His–Tyr mutant" (second number) in different redox and ligand states

	[Å]				[°]
	D(Cu-H240)	D(Cu-H290)	D(Cu-H291)	D(Cu-L)	ϕ(H290-Cu-L)
Cu[I]–YOH	1.96/1.96	2.18/2.22	1.98/1.96	–/–	–/–
Cu[I]–H_2O YOH	2.00/1.99	2.19/2.26	2.01/1.99	2.36/2.41	104.62/95.11
Cu[I]–H_2O YO^-	1.97/2.02	2.26/2.28	1.99/2.03	2.43/2.34	95.08/110.64
Cu[II]–YOH	1.94/1.96	1.99/2.06	1.95/1.96	–/–	–/–
Cu[II]–OHYOH	2.06/2.05	2.07/2.07	2.05/2.06	1.85/1.86	150.14/149.91
Cu[II]–H_2OYOH	1.98/2.00	2.00/2.12	1.98/1.99	2.08/2.37	146.95/99.99
Cu[II]–OH YO*	2.08/2.05	2.07/2.07	2.04/2.05	1.85/1.86	151.48/166.90
Cu[II]–OH YO^-	2.04/2.02	2.08/2.08	2.05/2.04	1.87/1.86	151.60/164.13
Cu[II]–H_2O YO^-	1.98/1.98	2.19/2.27	2.00/1.98	2.40/2.39	99.64/94.6

via structural constraints; the carbons of the terminal methyl groups of the peripheral peptide bonds of the amino acid residues surrounding the metal centers were fixed to their position in the crystal structure. The effect of the covalent bond between His-240 and Tyr-244 was studied by optimizing the Cu_B system in the various redox and ligand states but without the crosslink, *i.e.,* by protonating the N_ε and C_ε atoms of His-240 and Tyr-244, respectively. The same optimization protocol was used for these *in silico* His–Tyr "mutant" systems as for the "wild type". Energetics, spin, and charge densities were evaluated by single point calculations using a TZVP basis set on all atoms.

Along the reaction cycle, two charges separate from the Cu_B center can be assumed to perturb the spin and charge distributions of the system: a negatively charged oxygenous ligand of heme a_3, and the positively charged protonated Lys-319 located in the K-channel. Their effects on the electronic structure of the state Cu[II]–H_2O Y–O^- were simulated by using a point charge model. The heme a_3 ligand was simulated by placing a point charge approximately 1.5 Å from the water ligand of copper, its magnitude being scaled from 0.0*e* to −1.0*e*. Protonated Lys-319 was simulated by a point charge located 10 Å from the phenolic oxygen of Tyr-244 in the direction of the K-channel. Single point energy calculations were performed, from which Mulliken spin and point charges were calculated.

A value of −109.5 kcal/mol was used as the energy of an electron reducing the Cu_B system. This energy corresponds to the redox difference between reduced and oxidized heme *a* [68]. A vacuum energy of −270.6 kcal/mol was used for the proton [69].

All quantum chemical calculations were performed with the TURBOMOLE v5.9 quantum chemistry package [70]. VMD [71] and gOpenMol [72,73] were used for visualization.

3. Results

3.1. Geometry of the Cu_B site during the catalytic cycle

The optimized Cu_B systems in different redox and ligand states closely resemble the available X-ray structures of CcO. For example, the root-mean-square deviation (RMSD) between all non-hydrogen atoms of Cu[II] YOH and the fully oxidized X-ray structure is 0.3 Å. For comparison, the RMSD between the fully oxidized and reduced X-ray structures of the Cu_B center in *B. taurus* CcO is 0.1 Å, while the RMSD between the X-rays structures of the Cu_B center from four different organisms is 0.3 Å [63,74–76].

Although there are some interesting redox-state dependent structural variations in the coordination of the copper (see below), the overall structural features of the optimized Cu_B systems are very similar to each other. The RMSD between all optimized structures is 0.18 Å (without hydrogens); if Cu[I] and Cu[II] states are compared separately, the RMSD is 0.06 Å and 0.15 Å, respectively.

The structural features of the Cu_B system are summarized in Table 2. For the Cu[I] states, the bond to His-290 is on average 0.23 Å longer than the two other His–Cu bonds (2.18–2.26 Å vs. 1.96–2.01 Å). For the corresponding Cu[II] structures, the histidines bind more symmetrically (all bonds 1.94–2.08 Å). This is in agreement with studies on inorganic cupric and cuprous complexes, in which the former prefer a trigonal coordination while the latter prefer tetragonal geometry [77]. EXAFS studies on the Cu_B center in CcO have also suggested a different coordination between the cuprous and cupric states [78]. A difference between Cu[I] and Cu[II] can also be observed in the angles of the bound ligand; the angle between His-290, Cu, and its OH or H_2O ligand is ~100° in the cuprous states while it is ~150° in the cupric states. A water ligand binds to Cu[I] and Cu[II] states with bond lengths of 2.36 Å and 2.08 Å, respectively, indicating that in the cuprous state the water molecule is more weakly bonded to the copper compared to the cupric state. The hydroxyl ligand has a characteristic bond length of 1.85–1.87 Å, which does not change significantly between the different states. The Cu[I]–OH Tyr–OH structure was found to be unstable, *i.e.,* the structure dissociates upon structure optimization, possible reasons for which will be discussed below. Interestingly, the Cu[II]–H_2O Y–O^- state seems to be an outlier among the Cu[II] states shown in Table 2, since its bond lengths are more reminiscent of a Cu[I] state (see below).

Apart from the dissociation of His-240 from Tyr-244 in the His–Tyr "mutant" systems, there are otherwise only minor structural changes in the coordination of the copper due to this modification (Table 2). In the Cu[II]–H_2O Y–O^- state, the bond between His-290 and Cu_B is 0.06 Å longer in the "mutant" compared to the "wild type". The Cu[I]–H_2O Y–OH state has also a somewhat longer Cu–water bond length in the "mutant" (0.05 Å), which is even more pronounced in Cu[II]–H_2O Y–OH (0.28 Å) (Table 2). The largest structural variation in the His–Tyr "mutant" takes place in Cu[I]–H_2O Y–O^- where the backbone hydrogen bonding between His-240 and Tyr-244 is somewhat longer compared to the other states, but is compensated by hydrogen bonding between the aquo ligand of the copper and Tyr-244. This structural variation is probably due to the lack of the His–Tyr bond, but does not affect the general conclusions of this work, as it is only found to take place in this structure.

3.2. Comparison of HOMO–LUMO gaps

The energy gap between highest occupied (HOMO) and lowest unoccupied molecular orbitals (LUMO) is a measure of the excitability, but gives also indication on the stability and chemical reactivity of the molecule. A low HOMO–LUMO gap usually indicates that the molecule is chemically less inert. HOMO–LUMO gaps of the different redox and ligand states from both the "wild type" and His–Tyr "mutant" systems are summarized in Table 3. The HOMO–LUMO gap for the Cu[I] structures are in general higher than for Cu[II] structures, indicating that cuprous structures are in general more inert than the cupric structures, which is typical for closed-shell molecules. As the Cu[I]–OH YOH dissociates upon structure optimization, the value reported in the table is calculated using the Cu[II]–OH YOH structure in a cuprous state.

Table 3
HOMO–LUMO gaps of the different redox and ligand states of Cu_B for the "wild type" and "His–Tyr mutant" systems

HOMO–LUMO gaps [eV]	"wild type"	"His–Tyr mutant"	$\Delta E_{HOMO-LUMO}$
Cu[I]–YOH	+4.73187	+5.30707	−0.57520
Cu[I]–OH YOH[a]	+1.98565	+2.14017	−0.15452
Cu[I]–H_2O YOH	+4.33454	+4.90886	−0.57432
Cu[I]–H_2O YO^-	+3.62566	+3.73859	−0.11293
Cu[II]–YOH	+0.58433	+0.38431	+0.20000
Cu[II]–OH YOH	+3.04741	+1.73419	+1.31322
Cu[II]–H_2OYOH	+1.32188	+0.34084	+0.98104
Cu[II]–OH YO*	+2.15990	+2.32996	−0.17006
Cu[II]–OH YO^-	+1.08038	+0.87172	+0.20866
Cu[II]–H_2O YO^-	+1.20223	+1.64323	−0.44100

[a] calculated in the Cu[II]–OH YOH structure.

For the cuprous structures the systems without the His–Tyr crosslink have larger gaps than the "wild type" structures, whereas the opposite holds for the cupric structures. The only exceptions in this trend are Cu[II]–OH YO* and Cu[II]–H_2O YO^-, which may be due an increased radical character in systems without the His–Tyr bond (see Section 3.3). The HOMO–LUMO gap for Cu[II]–H_2O YOH in the His–Tyr "mutant" is very similar to the HOMO–LUMO gap of the unligated model, which is in agreement with the long water–copper distance (2.4 Å, Table 2).

3.3. Spin distributions

The spin populations of the cupric states are shown in Fig. 3 and summarized in Table 4. In the Cu[II]–OH YOH, Cu[II]–H_2O YOH, and Cu[II]–OH Y–O^- states, the unpaired electron is delocalized over the copper atom, the histidine nitrogens and the oxygenous ligand, and approximately 60% of the spin resides on the copper atom itself (Table 4). The Cu[II]–OH Y-O* state with $S=1$ shows a similar spin distribution around the copper as in the $S=1/2$ systems, but in addition, 95% of the spin of the second electron is localized at the tyrosine ring, as expected. The spin of an unpaired electron also delocalizes somewhat (~15%) to the tyrosine moiety when no oxygenous ligand is bound to the copper (Cu[II] YOH). In general, if a system has no natural location for excess spin, it will lead to scattering of the spin distribution over a large area (see Section 3.4).

Table 4
Comparison of the spin densities between "wild type" and "His–Tyr mutant" systems

	H240	Y244	H290	H291	Cu	L	Gross-SD
Cu[II] YOH	9.6/3.0	15.2/54.6	13.5/6.3	6.4/2.8	55.3/33.2	0.0/0.0	1.14/1.12
Cu[II]–OH YO*	9.4/6.8	95.6/100	4.4/5.4	7.2/7.8	61.6/58.8	21.8/21.2	2.50/2.57
Cu[II]–OH YO^-	7.0/8.4	0.0/0.0	4.1/5.1	6.9/7.2	62.4/57.8	19.7/21.4	1.09/1.12
Cu[II]–H_2O YO^-	3.7/0.0	95.0/100	0.0/0.0	0.0/0.0	1.4/0.0	0.0/0.0	1.42/1.46
Cu[II]–H_2O YOH	9.2/4.3	0.0/33.7	12.6/7.6	8.9/4.1	66.1/50.3	3.2/0.0	1.09/1.10
Cu[II]–OH YOH	6.4/6.9	0.0/0.0	4.4/4.3	7.0/6.8	61.2/58.1	21.1/23.9	1.10/1.11

The amount of (Mulliken) spin density is divided into subsystems: The histidine residues H-240, H-290 and H-291; the tyrosine Y-244; the copper ion Cu; the ligand to copper, L. The integrated gross spin density is also reported (gross SD). The first and second numbers indicate [%] of total spin on "wild type" and "His–Tyr mutant" systems, respectively.

The Cu[II]–H_2O Y–O^- state shows an aberrant spin distribution, as already indicated by its geometrical properties (Fig 3). The spin of the unpaired electron in this $S=1/2$ system resides to 95% on the tyrosine, which indicates that the Cu[I]–H_2O Y-O* resonance form is dominant. Note that this is not the case for Cu[II]–OH Y-O^- where the spin lies

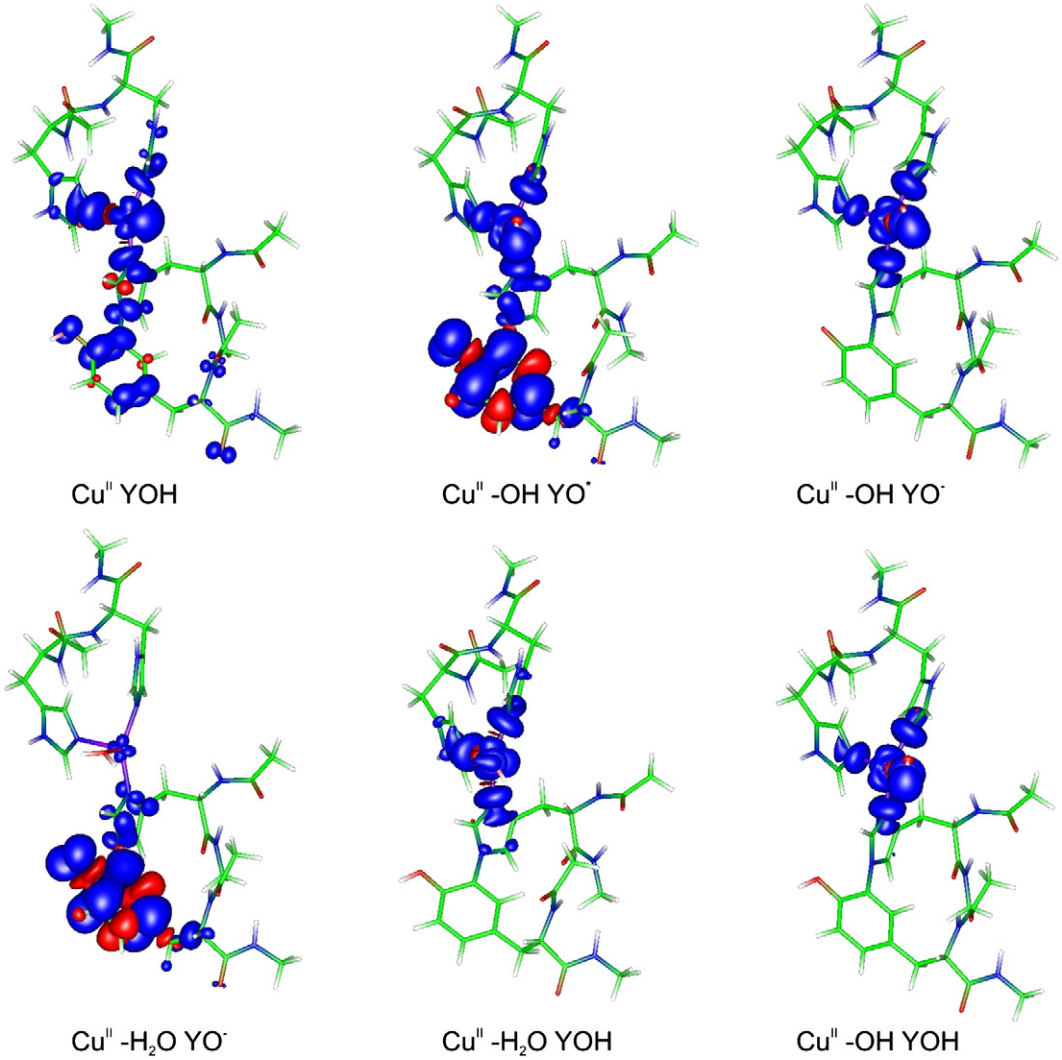

Fig. 3. Spin distributions of the "wild type" system. Blue regions represent excess α spin density and red regions excess β spin density. Isocontour values of 0.01*e* and −0.01*e* have been used for the α and β spin densities, respectively.

entirely on the copper and its immediate surroundings. However, in Cu[II]–H_2O Y-O^- a small fraction of the spin (~1%) is nevertheless on the copper and some on His-240 (~4%), which indicates that this state is not a pure Cu[I] state either. The half-and-half functional, BHLYP [54,55], which contains 50% HF-exchange, gives qualitatively a similar description as obtained with the B3LYP functional, although at the BHLYP level, the spin distribution is somewhat more localized on Tyr-244 (97%). This is reassuring, as it has been suggested that B3LYP in some cases tends to underestimate the spin populations of copper [79]; here, this is not the case.

The corresponding spin populations of the His–Tyr "mutant" are shown in Fig. 4 (see also Table 4). Compared to the "wild type", the spin is now generally more localized, either to the region around the copper or to the tyrosine ring. This trend may be expected as the His–Tyr bond connects the electronic systems of the aromatic phenol and imidazole rings. Comparison of Cu[II]–H_2O Y–O^- in the "wild type" and His–Tyr "mutant" indicates another function of the bond: while an electronic equilibrium between the two resonance forms (Cu[I]/Tyr-O* ↔ Cu[II]/Tyr-O^-) can be observed in the "wild type", the radical form is more dominant in the "mutant" in which the complete spin of the unpaired electron resides on the phenol moiety. Hence, the His–Tyr bond destabilizes the radical of Tyr, and therefore increases the relative electron affinity of Tyr (cf. section V). The spin of the second electron in Cu[II]–OH Y-O* of the "mutant" is similarly completely localized to the phenol. Finally, the spin distribution in the Cu[II]–H_2O Y–OH state is very different in the His–Tyr "mutant" compared to the "wild type"; the unpaired electron in the "mutant" delocalizes all over the system, resembling the spin distribution in the unligated state. This is probably due to the relatively long bond distance between the copper and its water ligand when the His–Tyr bond is absent (Table 2). This is also supported by a similar HOMO–LUMO gap (Table 3) of this structure compared to the unligated structures. Care was taken to assure that this unexpected spin distribution is not, for example, due to convergence to an excited state. Tighter convergence thresholds and denser grids for the DFT quadrature lead to the same state. Also, the lowest excitation energy out of this state was confirmed to be positive. Although convergence to the global minimum can never be rigorously ensured, we find no indication of the opposite.

Further insight into the spin distributions was obtained by studying the amount of spin polarization in the different ligand states. This was done via the gross spin density, that is, the sum of unpaired α and β spin densities in the systems, as reported in Table 4. A few points are worth noting. First, all open-shell systems exhibit spin-polarization to a certain degree. For most systems, the gross spin density is *ca.* 10% higher than the net spin density, much smaller than what is found

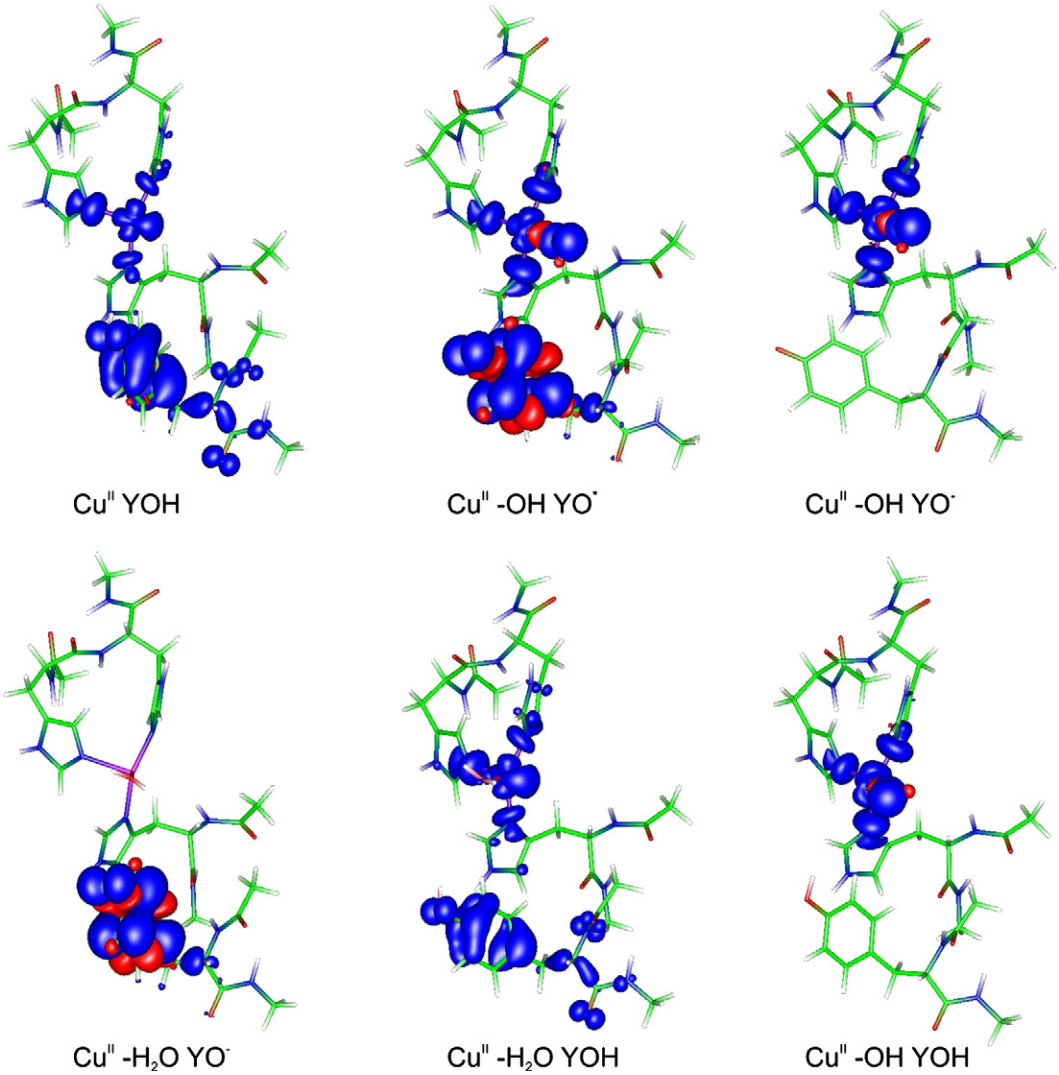

Fig. 4. Spin distributions of the His–Tyr "mutant" system. Blue regions represent excess α spin density and red regions excess β spin density. Isocontour values of 0.01*e* and −0.01*e* have been used for the α and β spin densities, respectively.

in, for example, low-spin iron porphyrins [51]. Two of the systems behave differently. The (formal) Cu[II]–H_2O Y–O^- state and the Cu[II]–OH Y-O* radical both contain an excess of roughly half an unpaired electron. As seen in Figs. 3 and 4, most of the polarization, expressed as presence of β-spin, manifests itself around the tyrosine carbons. This further corroborates the view that here, Cu[II]–H_2O Y–O^- is more correctly described as a Cu[I]–H_2O Y-O* radical.

Comparing the "wild type" and "mutant" systems, some differences in the degree of spin polarization are seen, but none are very large. We also emphasize that spin contamination is insignificant, and not the source of the polarization. At the B3LYP level, the doublet states have $\langle S^2 \rangle$ values of 0.75–0.77, and the triplet states a value of 2.03, while the pure, non-polarized expectation values are 0.75 and 2, respectively.

3.4. Charge density differences

Fig. 5 shows the difference in charge densities between cuprous and cupric states for the "wild type" system, calculated in the geometries of the cupric states. In Fig. 6, the corresponding differences are shown in the absence of the His–Tyr crosslink (see also Table 5). When compared to Figs. 3 and 5, and as observed previously [50,51], it is seen that the localization of charge and spin densities do not always coincide.

In the $\mathbf{P_M} \rightarrow \mathbf{P_R}$ transition *i.e.* Cu[II]–OH Y-O* → Cu[II]–OH Y–O^-, the charge of the incoming electron spreads according to the population analysis as follows: 82% to Tyr-244, 12% to His-240, and the remaining 6% to the copper and its two other histidine ligands. In the corresponding His–Tyr "mutant", 98% of the additional charge upon reduction is found on the tyrosine ring, indicating that charge flows through the His–Tyr bond from Tyr-244 to His-240.

The Cu[II]–H_2O Y–O^- → Cu[I]–H_2O Y–O^- transition may occur in the $\mathbf{O_H} \rightarrow \mathbf{O_{H,R}}$ step of the catalytic cycle (Fig. 2). In accordance with the aberrant spin distribution in Cu[II]–H_2O Y–O^-, where most of the unpaired spin is on the tyrosine (see above), Tyr-244 accepts 79% of the charge of the electron while His-240 accepts 14%. The His–Tyr bond seems to play a similar role as in the previous transition; in the His–Tyr "mutant", 83% and 7% of the added charge localize on Tyr-244 and His-240, respectively.

In the Cu[II]–H_2O Y–OH → Cu[I]–H_2O Y–OH transition, the charge of the incoming electron localizes quite symmetrically around the copper atom (Table 5), while only 8% of the charge localizes on Tyr-244. In the His–Tyr "mutant", ~30% of the charge, which in the "wild type" system resides on His-290, His-291 and the water ligand, is transferred to Tyr-244. Also here the His–Tyr bond seems to work as a wire for the spreading out charge.

Cu[II]–OH Y–OH → Cu[I]–OH Y–OH is a hypothetical transition as the latter state was found to be unstable. The instability can be understood from the charge density difference plot; the hydroxy ligand accumulates extensive negative charge around the copper, which cannot be stabilized by the cuprous metal. The charge spreads

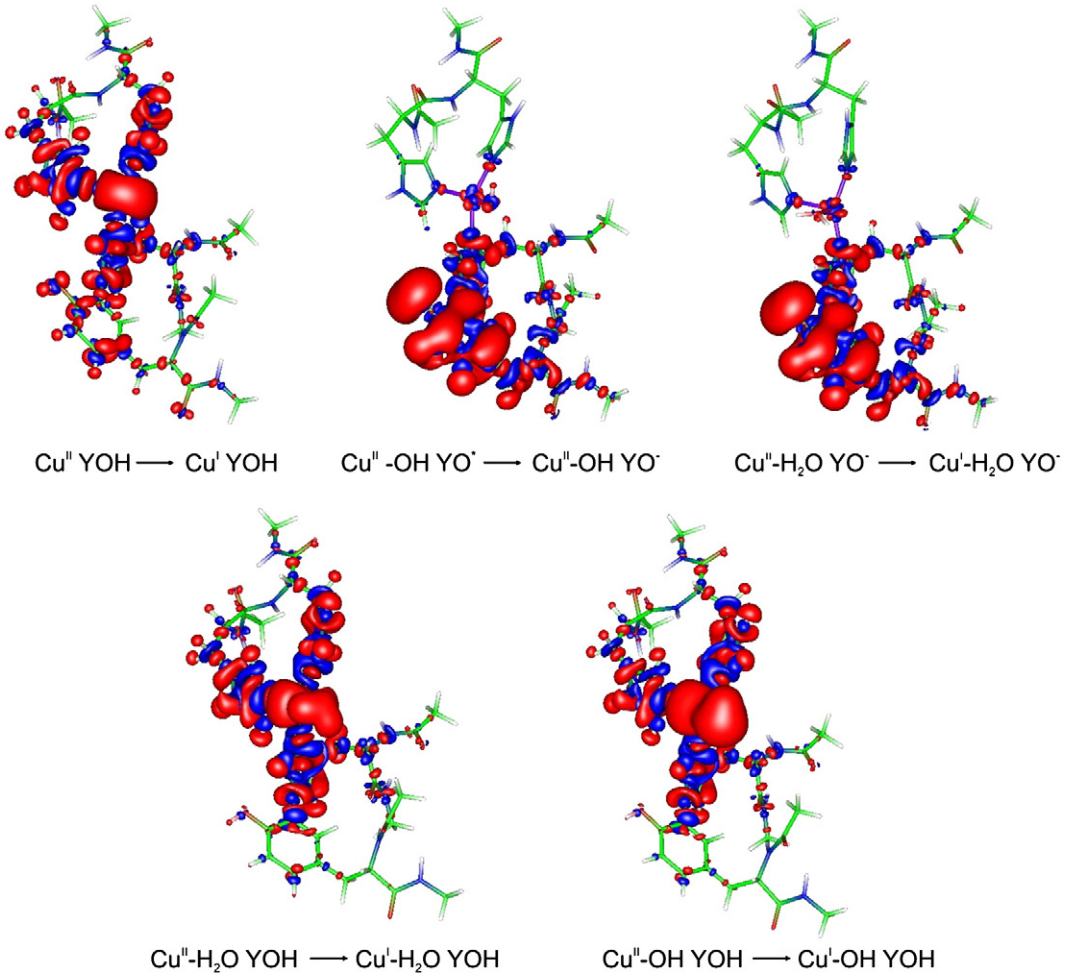

Fig. 5. Charge density differences in the *wt* system. Blue regions represent excess positive charge (less electron density) and red regions excess negative charge (higher electron density) between reduced and oxidized structures. Isocontour values of 0.01*e* and −0.01*e* have been used for the low and high electron density, respectively.

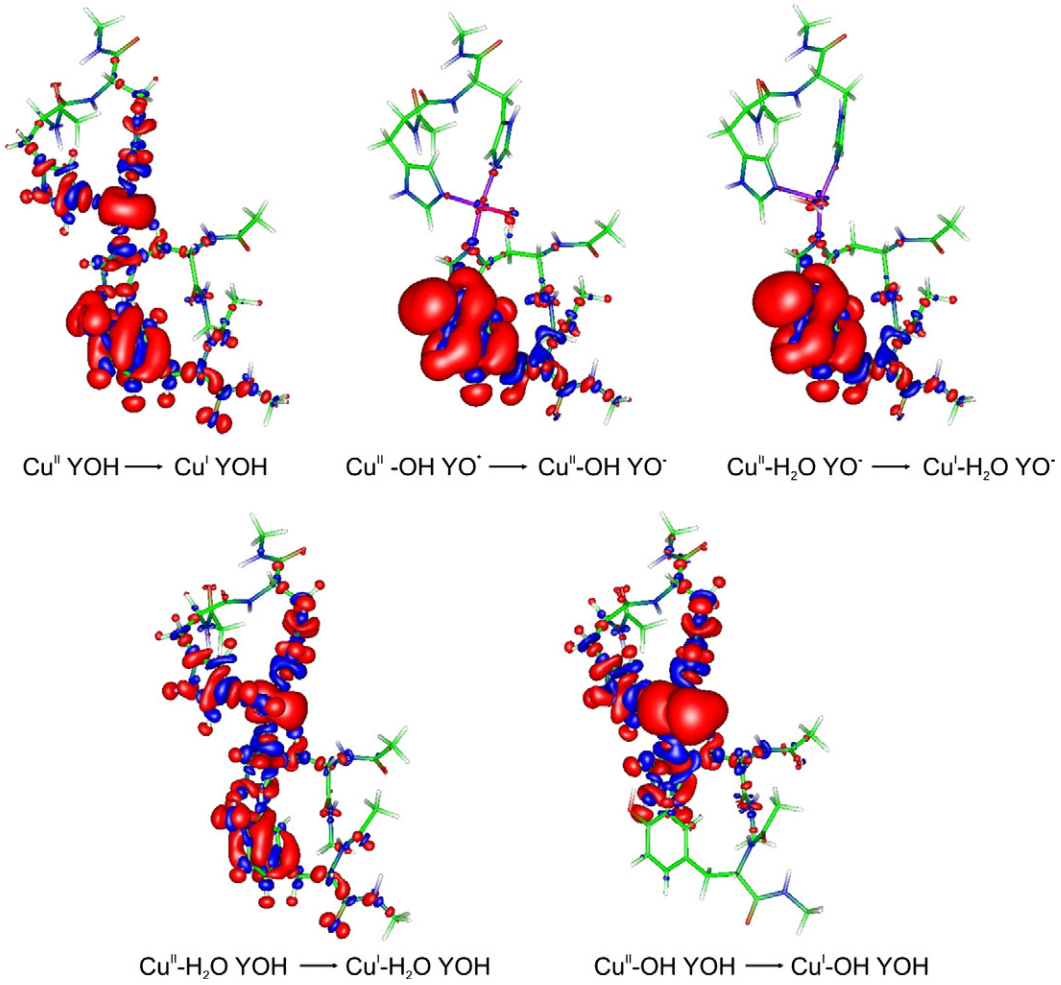

Fig. 6. Charge density differences in the His–Tyr "mutant" system. Blue regions represent excess positive charge (less electron density) and red regions excess negative charge (higher electron density) between reduced and oxidized structures. Isocontour values of 0.01*e* and −0.01*e* have been used for the low and high electron density, respectively.

quite symmetrically around the copper atom and its ligands, and is similar in the "wild type" (Fig. 5) and His–Tyr "mutant" (Fig. 6) systems.

3.5. Thermodynamic importance of the His–Tyr bond

Energy level diagrams of the different redox and ligand states of Cu_B are summarized in Fig. 7a for the "wild type" and in Fig. 7b for the His–Tyr "mutant". All transitions are relative to the energy of Cu [II]–OH Y-O*. In addition, the energetics discussed below represent only the internal energetics of the Cu_B center, without heme a_3. In many transitions of the binuclear site, *e.g.* $\mathbf{P_M}\rightarrow\mathbf{P_R}$, $\mathbf{P_R}\rightarrow\mathbf{F}$, and $\mathbf{O}\rightarrow\mathbf{E}$, the structure of heme a_3 remains unchanged (within the current model, Fig. 2). Therefore it seems justified to draw parallels between the properties of the Cu_B site and the binuclear site. In addition, we consider that the contribution of heme a_3 would be the same on the Cu_B center for the "wild type" and the His–Tyr "mutant" systems.

Table 5
Comparison of the charge density differences between oxidized and reduced systems ([II]/[I] or TyrO*/TyrO⁻) for the "wild type" and "His–Tyr mutant", respectively

	H240	Y244	H290	H291	Cu	L
Cu[II]–OH Y-O*/–	12.0/−0.9	82.0/97.6	1.4/1.1	2.0/0.6	1.7/1.0	0.9/0.5
Cu[II]/[I]–H_2O Y–OH	14.5/15.4	7.8/32.4	31.9/22.5	26.3/16.0	6.3/10.3	13.2/3.4
Cu[II]/[I]–H_2O Y–O^-	14.4/6.9	79.3/82.8	3.2/1.6	0.2/5.5	3.7/−2.9	−0.8/6.1
Cu[II]/[I]–OH Y–OH	15.0/19.6	5.6/1.4	20.2/19.5	21.4/20.5	12.8/12.7	25.0/26.3
Cu[II]/[I] YOH	18.3/9.8	20.5/53.3	30.6/17.5	20.0/10.7	10.6/8.7	0.0/0.0

The amount of charge is divided into subsystems: The histidine residues H-240, H-290 and H-291; the tyrosine Y-244; the copper ion Cu; the ligand to copper, L. The first and second numbers indicate the distribution of one electron charge on the subsystems in [%] for the "wild type" and "His–Tyr mutant" systems, respectively.

The first transition shows that for the "wild type" system the reduction of the Tyr-radical in Cu[II]–OH Y-O* (the $\mathbf{P_M}$ state) is slightly endergonic (+2.8 kcal/mol). The prior $\mathbf{A}\rightarrow\mathbf{P_M}$ transition (Fig. 2) was not considered in this work, but it is known experimentally to go to completion. Using an experimental error marginal of 1%, this means that this transition must be downhill by at least 2.8 kcal/mol. Blomberg *et al.* have estimated the $\mathbf{A}\rightarrow\mathbf{P_M}$ transition to be exergonic by 5.0 kcal/mol [80], which implies that the $\mathbf{A}\rightarrow\mathbf{P_R}$ transition has a total energy drop of 2.2 kcal/mol (−5.0+2.8 kcal/mol).

In contrast, reduction of $\mathbf{P_M}$ is far more costly in the His–Tyr "mutant" (+12.0 kcal/mol; Fig. 7b), so that the $\mathbf{P_R}$ state is energetically much more difficult to reach without the His–Tyr bond. This suggests that the His–Tyr crosslink increases the electron affinity of Tyr-244 by *ca.* 0.4 eV in the $\mathbf{P_M}$ state (12.0–2.8 kcal/mol=9.2 kcal/mol ~0.4 eV). The overall energetics of $\mathbf{A}\rightarrow\mathbf{P_R}$ is also changed. During $\mathbf{A}\rightarrow\mathbf{P_M}$ the Cu_B center undergoes a Cu[I] Y–OH→Cu[II]–OH Y-O* transition. In the His–Tyr "mutant" this transition is 3.3 kcal/mol more stable compared to the "wild type" system. Furthermore, if it is assumed that the contribution of heme a_3 would be the same for both "wild type" and

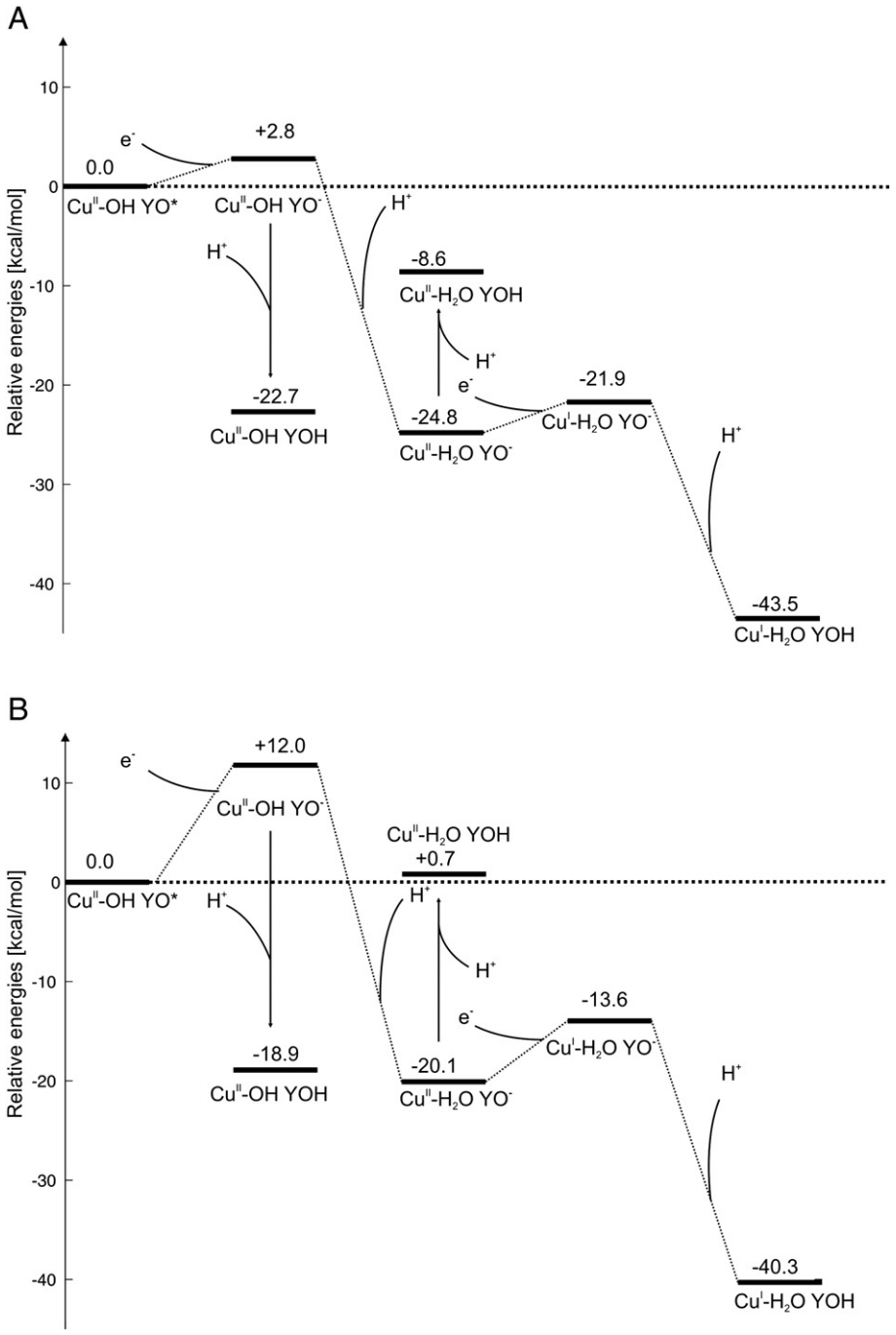

Fig. 7. Energy level diagrams for (A) the *wt* system, and (B) the His–Tyr "mutant" system.

"mutant" system during $\mathbf{A}\rightarrow\mathbf{P_M}$, this suggest that the overall $\mathbf{A}\rightarrow\mathbf{P_R}$ is endergonic by 3.7 kcal/mol (−5.0−3.3+12.0 kcal/mol) in the "mutant", whereas this transition is exergonic by 2.2 kcal/mol in the "wild type" (see above). Thus the His–Tyr bond has an important function in favoring O–O bond cleavage, and in formation of the $\mathbf{P_R}$ state.

Protonation of the $\mathbf{P_R}$ state (Cu[II]–OH Y–O^-) yields state **F** (Fig. 2). Here, protonation of the hydroxyl ligand of copper is favored over protonation of Tyr-244 by 2.1 kcal/mol (27.6–25.5 kcal/mol, Table 6), in agreement with the difference in optical spectrum between the two species (see Introduction), and recent infrared data, which suggest that Tyr-244 is anionic in state **F** [31]**.** The observed energetic preference for the Cu[II]–H_2O Y–O^- structure over Cu[II]–OH Y–OH also circumvents formation of the unstable Cu[I]–OH Y–OH species upon reduction by the next electron. As shown in Fig. 7A,B, Tyr-244 has a weak proton affinity in the preferred **F** state (Cu[II]–H_2O Y–O^-; Fig. 7A,B, −24.8−(−8.6) kcal/mol=16.2 kcal/mol). However, when this state is reduced to Cu[I]–H_2O Y–O^-, the tyrosinate acquires a very high proton affinity (−43.5−(−21.9) kcal/mol=−21.6 kcal/mol), and will easily attract a proton via the K-channel (see Discussion).

In the **F** state of the "mutant" system, the energetic preference for protonating Tyr-244 over the hydroxyl ligand of the copper is lowered to 1.2 kcal/mol (32.1–30.9 kcal/mol, Fig. 7b, Table 6). The reason is that the proton affinities of both Tyr-244 and the oxygenous copper ligand increase compared to the "wild type" system, but the proton affinity (PA) of Tyr-244 increases somewhat more. The proton affinity of Tyr-244 in the preferred **F** state (Cu[II]–H_2O Y–O^-) is even lower than in the "wild type" system (20.8 kcal/mol vs. 16.2 kcal/mol in the "wild type"), probably due to the very weak bond between the water and

Table 6
The effect of the His–Tyr bond on electron and proton affinities of the system

Electron affinities			
Tyr:	"wild type"	"His–Tyr mutant"	ΔEA[kcal/mol]
Cu[II]–OH–YO$^-$→Cu[II]–OH–YO*+e$^-$	−2.8	−12.0	+9.2
Cu[I]–YOH→Cu[II]–OH–YO*+e$^-$	–	–	+3.3
Cu:			
Cu[I]–H_2O YOH→Cu[II]–H_2O YOH+e$^-$	+34.9	+41.0	−6.1
Cu[I]–H_2O YO$^-$→Cu[II]–H_2O YO$^-$+e$^-$	−2.9	−6.5	+3.6
Cu[I] YOH→Cu[II] YOH+e$^-$	+48.4	+48.7	−0.3
Proton affinities			
Tyr:	"wild type"	"His–Tyr mutant"	ΔPA[kcal/mol]
Cu[II]–OH YOH→Cu[II]–OH YO$^-$+H$^+$	+25.5	+30.9	−5.4
Cu[II]–H_2O YOH→Cu[II]–H_2O YO$^-$+H$^+$	−16.2	−20.8	+4.6
Cu[I]–H_2O YOH→Cu[I]–H_2O YO$^-$+H$^+$	+21.6	+26.7	−5.1
Cu–L:			
Cu[II]–H_2O YOH→Cu[II]–OH YOH+H$^+$	−14.1	−19.6	+5.5
Cu[II]–H_2O YO$^-$→Cu[II]–OH YO$^-$+H$^+$	+27.6	+32.1	−4.5

copper in Cu[II]–H_2O Y–OH (see Table 2). As for the $\mathbf{P_M}$ state, the reduction of **F** (Cu[II]–H_2O Y–O$^-$) is more costly without a His–Tyr bond (6.5 kcal/mol vs. 2.9 kcal/mol in "wild type"). However, as for the "wild type" system, Cu[I]–H_2O Y–O$^-$ is a state with a very high proton affinity (Fig. 7a,b, −40.3−(−13.6) kcal/mol=−26.7 kcal/mol).

Table 6 summarizes the differences in proton and electron affinities (EA) for the "wild type" and the His–Tyr "mutant" systems. The PA and EA values involving the Cu[II]–H_2O Y–O$^-$ state are complicated by the energetics of the Cu[II]→Cu[I] transition. For example, reduction of Cu[II]–H_2O Y–O$^-$ to Cu[I]–H_2O Y–O$^-$, reflects both the reduction of the Tyr-radical to a tyrosinate, and the partial reduction of a cupric state to a cuprous state. In contrast, in the His–Tyr "mutant", this transition is a rather pure reduction of a tyrosine radical (see Section 3.3, and Fig. 4). Interestingly, in the "mutant" the reduction of the Tyr-radical requires significantly more energy if the copper binds a hydroxyl instead of a water molecule (+12.0 kcal/mol, and 6.5 kcal/mol, respectively). This indicates that without the His–Tyr bond, the electrostatic effect of the copper ligand is rather large. However, in the "wild type" system the energy for reduction of the Tyr radical is nearly the same whether the copper binds a water molecule or a hydroxyl group (2.8 kcal/mol, and 2.9 kcal/mol, respectively). This indicates that the negative charge of the phenolate delocalizes to a larger area due to the crosslink, decreasing the electrostatic repulsion between the hydroxyl and phenolate (Figs. 3 and 4).

3.6. Environmental effects on the electronic structure of Cu[II]–H_2O Y–O$^-$

The analysis carried out above has been restricted to an isolated albeit relatively large system around the Cu_B site. One unexpected finding was the spin and charge distribution of the formal Cu[II]–H_2O Y–O$^-$ state, in which the spin was found to be largely localized to the tyrosine with predominantly cuprous Cu_B. This structure of the Cu_B system is expected for both states **F** and $\mathbf{O_H}$ in the catalytic cycle (Fig. 2). It was therefore of interest to test how this state might be perturbed by an oxygenous axial ligand on heme a_3 iron, and a positive charge on the Lys-319 in the K-channel of proton transfer that eventually leads to the crosslinked Tyr-244. The effect of a negatively charged distal axial ligand of heme a_3 on the spin and charge distribution of the Cu[II]–H_2O Y–O$^-$ state is shown in Fig. 8. When the magnitude of the point charge is scaled from 0.0*e* to −1.0*e*, the spin distribution between the copper and Tyr-244 changes from 1/95 to 17/73. Similarly, the negative charge on the Tyr increases from 0.0*e* to −0.19*e*, indicating stabilization of the Cu[II]/Tyr-O$^-$ resonance form. The aim with this point charge perturbation is not as such to model the effect of heme a_3, but rather to study the "maximal" perturbation effect heme a_3 might have on the spin and charge distributions of Cu[II]–H_2O Y–O$^-$.

If a positive charge is placed 10 Å away from Tyr-244 (see Models and methods), simulating a positively charged lysine-319 in the K-pathway, the spin and charge distributions are perturbed dramatically (Fig. 8). Even without the negative charge near the Cu, 62% of the spin resides on the copper, and the charge of Tyr is −0.87*e* indicating a clear phenolate character (for comparison, the charge of Tyr is −0.9*e* in Cu

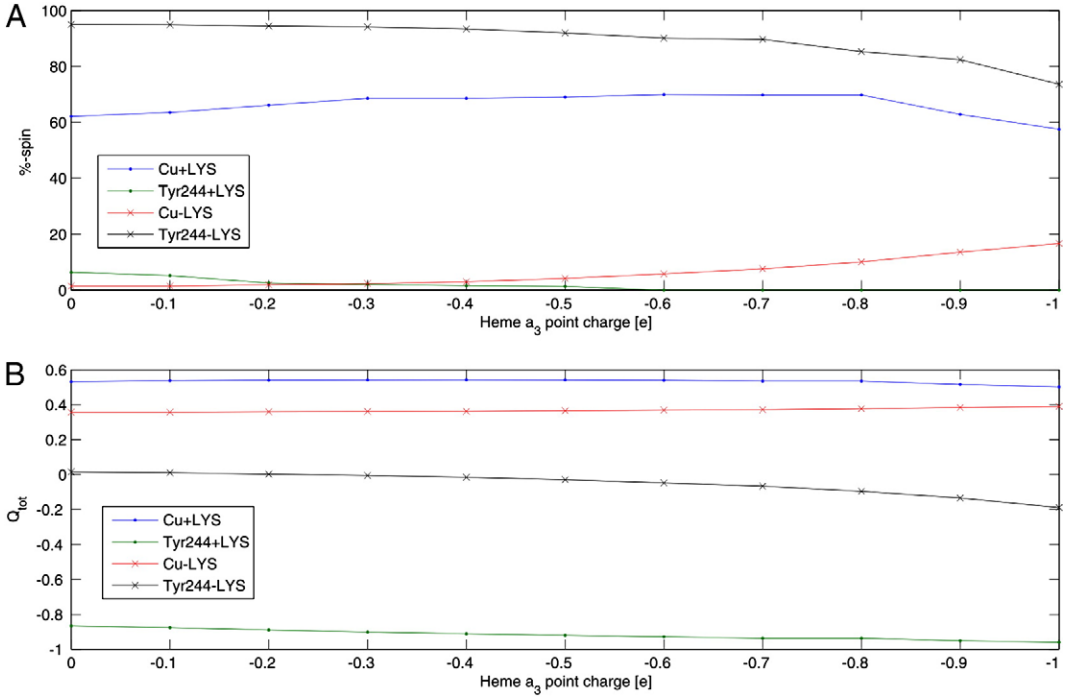

Fig. 8. Spin (A), and Mulliken charges (B) of Cu and Tyr-244 when the point charge of the negative oxygenous ligand of heme a_3 is scaled from 0.0*e* to −1.0*e* with (+LYS) and without (−LYS) Lys-319.

[II]–OH YO$^-$ and 0.0*e* in Cu[II]–OH YO*), and in this case the negative charge near the copper does not enhance this effect much further (Fig 8A and B). This point charge effect indicates that the relative redox potentials of the copper and the Tyr may be easily perturbed by an electrostatic field which alters the electronic state of the Cu_B site (for comparison, two unit point charges 10 Å apart have an interaction energy of ~8 kcal/mol if the dielectric constant is 4).

From Table 4 it may be roughly estimated that the midpoint redox potential (E_m) of the copper is 190 mV higher than the E_m for tyrosine in the formal Cu[II]–H_2O Y–O$^-$ state (which makes it appear more as a Cu[I]–H_2O Y-O* state). A positive charge at lysine-319 changes the ΔE_m to ~80 mV the tyrosine now having the higher potential (Fig. 8), an effect of 270 mV. This is a reasonable electrostatic effect over 10 Å as it predicts a mean effective dielectric constant of ~5 between the lysine and the tyrosine.

4. Discussion

The His–Tyr crosslink works as a wire for spreading out the charge in the Cu_B system, as indicated by the charge density analysis (see Figs. 5 and 6, and Table 5). Some of the charge of Tyr-244 is transferred to His-240, which causes Tyr-244 to become less negative and weakens the electrostatic attraction between the phenolic proton of Tyr and the ring, lowering its proton affinity. For the same reason there is no energetic difference with respect to reduction of the Tyr radical in the "wild type" system, whether the copper binds a hydroxyl or a water molecule (see above). The increase in electron affinity of Tyr-244 due to the crosslink can also be understood in terms of electron delocalization; the repulsion between a negatively charged surface and a negatively charged particle is stronger if the surface charge is concentrated to a smaller area. The removal of an electron from a system with a high charge delocalization, such as the "wild type" system, requires more energy compared to a situation where the charge is more localized, as in the His–Tyr "mutant". The increased electron delocalization facilitated by the His–Tyr crosslink thus leads to a larger electron affinity and a smaller proton affinity of the Tyr moiety than for the His–Tyr "mutant" without the connecting bond.

The energetics of protonating Tyr-244 can be understood from the charge density distribution of the system. When the Cu[II]–H_2O Y–O$^-$ state is reduced, negative charge accumulates on Tyr, which drastically increases its proton affinity. This could explain why the K-channel is not utilized for proton uptake prior to the $\mathbf{E_H}$ state, in which cuprous copper appears for the first time (see Fig 2). In the $\mathbf{E_H \rightarrow E_{H,R}}$ transition, reduction of Fe[III]–OH yields a highly unstable Fe[II]–OH species, which must immediately accept a proton. Since the aqueous ligand of Cu[I] cannot provide this proton due to the instability of the cuprous hydroxide (see above), the proton is donated by Tyr-244, which reforms state Cu[I]–H_2O Y–O$^-$. The observed high pK_a of Tyr-244 in this state attracts a proton from the K-channel, producing the **R** state, thus closing the reaction cycle. These findings suggest the following function of the proton-conducting K-channel. Analogously to the proposed function of Tyr-244 as the proton donor in the $\mathbf{A \rightarrow P_R}$ transition where the O–O bond is broken, Tyr-244 donates a proton to the oxygenous ligand of the heme a_3 iron in the reductive phase of the catalytic cycle. Moreover, when the proton affinity of Tyr-244 is high, it can only be (re)-protonated from the K-channel. As suggested by MD-studies [11], Glu-242 is the proton donor for the oxygenous ligand of the copper in the oxidative phase, where the K-channel is not used for proton uptake. This suggests that the D-channel conducts the "chemical" proton for the oxygenous copper ligand, whereas the K-channel conducts protons to the distal heme a_3 ligand.

Recent FTIR experiments have suggested that Tyr-244 is deprotonated in the $\mathbf{P_R}$ and **F** states and at least partially in the $\mathbf{O_H}$ state [31]. The 1308 cm^{-1} vibration seen in these experiments indicates that Tyr-244 is in the phenolate and not the radical form, which seemingly contradicts our observation that the structure Cu[II]–H_2O Y–O$^-$ (in states **F** and $\mathbf{O_H}$) favors the cuprous-tyrosine radical resonance form. However, the observed perturbation of the electronic equilibrium between the copper and Tyr by protonation of Lys-319 may explain this discrepancy. The point charge effect of Lys-319 on the electronic structure of Cu_B may be of central importance in introducing coupling between the protonation state of the K-channel and the thermodynamic properties of Cu_B. Lepp *et al.* recently reported that mutation of Lys-319 to a methionine slows down the $\mathbf{A \rightarrow P_R}$ transition from 30 to 90 μs [81]. Our analysis showed that the positively charged Lys-319 stabilizes the anionic tyrosinate, which may explain this observation.

Although we have shown how different redox and ligand states influence the electron and proton affinities of the Cu_B site, and suggested a possible explanation to why the K-channel is activated in the second half of the reaction cycle, there are still many open questions concerning the Cu_B site, for example, the difference between the $\mathbf{O}_H$ and **O** states [82,83]. So far, no spectroscopic differences have been found between these states [84], although reduction of the former is coupled to proton-pumping while the latter is not. The relaxation of $\mathbf{O}_H$ to **O** occurs spontaneously, in the absence of an external electron donor. Since the Cu_B center is spectroscopically invisible in most states, the difference between $\mathbf{O}_H$ and **O** might be found in the structure of this center. It has been suggested that the redox potential of Cu_B is too low in the **O** state to drive proton translocation [3]. One possible explanation might be the coordination of the Cu_B site; cuprous complexes prefer a trigonal coordination, whereas cupric complexes prefer a tetragonal one. Therefore, a cupric complex of trigonal geometry is expected to have a high E_m. The (formal) Cu[II]–H_2O Y–O$^-$ state was shown to have a geometry more reminiscent of Cu[I] complexes due to the dominant Cu [I]–H_2O Y-O* resonance form. It was also shown that the electronic structure of this state is affected by environmental effects, such as a positive charge in the K-channel, which might also change the coordination of the copper. It is therefore possible that the $\mathbf{O}_H$ to **O** transition is linked to the protonation state of the K-channel. Calculations are currently in progress to study this connection more thoroughly.

5. Conclusions

Quantum chemical theory has been applied to describe the electronic structure and energetics of the Cu_B site in cytochrome *c* oxidase when cycling through different redox and ligand states. By energetic considerations, it may be understood why two different proton-conducting channels are used in the first and latter part of the cycle. It was suggested that the appearance of a high proton affinity of the tyrosinate in the Cu[I]–H_2O Y–O$^-$ state triggers proton transfer from the K-channel to Tyr-244 in the $\mathbf{O_H \rightarrow O_{H,R}}$ transition. The K-channel is not used in proton transfer prior to the $\mathbf{O_H}$ state because the proton affinity of Tyr-244 is very low as long as Cu_B is in the cupric form. *In silico* mutations were done to reveal the importance of the unique His–Tyr bond. It was shown that this bond, which links the aromatic systems of His-240 and Tyr-244, has a crucial effect on the function of the enzyme. It lowers the proton affinity of Tyr-244 and increases its electron affinity, thereby favoring O–O bond scission during catalysis. The bond also affects the copper, decreasing the proton affinity of its oxygenous ligand.

Acknowledgements

Prof. P.R. Taylor and Dr. Michael I. Verkhovsky are acknowledged for critical comments and enlightening discussion. The authors wish to acknowledge Prof. Margareta Blomberg for helpful advice. This work was supported by grants from the Sigrid Juselius Foundation, Biocentrum Helsinki, HENAKOTO and the Academy of Finland. It is also supported by the Academy of Finland through its Centers of Excellence Programme 2006-2011. The research collaboration is supported by the Nordic Center of Excellence in Computational Chemistry (NCoECC) project funded by NordForsk (070253). CSC – The Finnish IT Center for Science provided computational resources. V.R.I.

K. is supported by the Finnish Cultural Foundation, and the Graduate School of Biotechnology and Molecular Biology. M.P.J. is supported by the Lundbeck Foundation.

Appendix A. Supplementary data

Supplementary data associated with this article can be found, in the online version, at doi:10.1016/j.bbabio.2009.01.002.

References

[1] M.K.F. Wikström, Proton pump coupled to cytochrome *c* oxidase in mitochondria, Nature 266 (1977) 271–273.
[2] G.T. Babcock, M. Wikström, Oxygen activation and the conservation of energy in cell respiration, Nature 356 (1992) 301–365.
[3] M. Wikström, Cytochrome *c* oxidase: 25 years of the elusive proton pump, Biochim. Biophys. Acta 1655 (2004) 241–247.
[4] S. Iwata, C. Ostermeier, B. Ludwig, H. Michel, Structure at 2.8 Å resolution of cytochrome *c* oxidase from *Paracoccus denitrificans*, Nature 376 (1995) 660–669.
[5] T. Tsukihara, H. Aoyama, E. Yamashita, T. Tomizaki, H. Yamaguchi, K. Shinzawa-Itoh, R. Nakashima, R. Yaono, S. Yoshikawa, The whole structure of the 13-subunit oxidized cytochrome *c* oxidase at 2.8 Å, Science 272 (1996) 1136–1144.
[6] J.P. Hosler, S. Ferguson-Miller, D.A. Mills, Energy transduction: proton transfer through the respiratory complexes, Annu. Rev. Biochem. 75 (2006) 165–187.
[7] G. Brändén, R.B. Gennis, P. Brzezinski, Transmembrane proton translocation by cytochrome *c* oxidase, Biochim. Biophys. Acta 1757 (2006) 1052–1063.
[8] I. Belevich, M.I. Verkhovsky, Molecular mechanism of proton translocation by cytochrome *c* oxidase, Antioxid. Redox Signal 10 (2008) 1–29.
[9] I. Belevich, D. Bloch, N. Belevich, M. Wikström, M.I. Verkhovsky, Exploring the proton pump mechanism of cytochrome *c* oxidase in real time, Proc. Natl. Acad. Sci. U. S. A. 104 (2007) 2685–2690.
[10] I. Belevich, M.I. Verkhovsky, M. Wikström, Proton-coupled electron transfer drives the proton pump of cytochrome *c* oxidase, Nature 440 (2006) 829–832.
[11] M. Wikström, M.I. Verkhovsky, G. Hummer, Water-gated mechanism of proton translocation by cytochrome *c* oxidase, Biochim. Biophys. Acta 1604 (2003) 61–65.
[12] M.H.M. Olsson, A. Warshel, Monte Carlo simulations of proton pumps: on the working principles of the biological valve that controls proton pumping in cytochrome *c* oxidase, Proc. Natl. Acad. Sci. U. S. A. 103 (2006) 6500–6505.
[13] M.R.A. Blomberg, P.E.M. Siegbahn, Quantum chemistry applied to the mechanisms of transition metal containing enzymes — cytochrome *c* oxidase, a particularly challenging case, J. Comput. Chem. 12 (2006) 1373–1384.
[14] D.M. Popovic, J. Quenneville, A.A. Stuchebrukhov, DFT/electrostatic calculations of pK(a) values in cytochrome *c* oxidase, J. Phys. Chem. B 109 (2005) 3616–3626.
[15] J. Xu, M.A. Sharpe, L. Qin, S. Ferguson-Miller, G.A. Voth, Storage of an excess proton in the hydrogen-bonded network of the d-pathway of cytochrome *C* oxidase: identification of a protonated water cluster, J. Am. Chem. Soc. 129 (2007) 2910–2913.
[16] E. Fadda, N. Chakrabarti, R. Pomès, Acidity of a Cu-bound histidine in the binuclear center of cytochrome *C* oxidase, J. Phys. Chem. B 109 (2005) 22629–22640.
[17] M. Svensson-Ek, J.W. Thomas, R.B. Gennis, T. Nilsson, P. Brzezinski, Kinetics of electron and proton transfer during the reaction of wild type and helix VI mutants of cytochrome bo_3 with oxygen, Biochemistry 35 (1996) 13673–13680.
[18] P. Ädelroth, M. Svensson-Ek, D.M. Mitchell, R.B. Gennis, P. Brzezinski, Glutamate 286 in cytochrome aa_3 from *Rhodobacter sphaeroides* is involved in proton uptake during the reaction of the fully-reduced enzyme with dioxygen, Biochemistry 36 (1997) 13824–13829.
[19] M.L. Verkhovskaya, A. Garcia-Horsman, A. Puustinen, J.L. Rigaud, J.E. Morgan, M.I. Verkhovsky, M. Wikström, Glutamic acid 286 in subunit I of cytochrome bo_3 is involved in proton translocation, Proc. Natl. Acad. Sci. U. S. A. 94 (1997) 10128–10131.
[20] A.A. Konstantinov, S. Siletsky, D. Mitchell, A. Kaulen, R.B. Gennis, The roles of the two proton input channels in cytochrome *c* oxidase from *Rhodobacter sphaeroides* probed by the effects of site-directed mutations on time-resolved electrogenic intraprotein proton transfer, Proc. Natl. Acad. Sci. U. S. A. 94 (1997) 9085–9090.
[21] V.R.I. Kaila, M.I. Verkhovsky, G. Hummer, M. Wikström, Glutamic acid 242 is a valve in the proton pump of cytochrome *c* oxidase, Proc. Natl. Acad. Sci. U. S. A. 105 (2008) 6255–6259.
[22] V.R.I. Kaila, M.I. Verkhovsky, G. Hummer, M. Wikström, Prevention of leak in the proton pump of cytochrome *c* oxidase, Biochim. Biophys. Acta 1777 (2008) 890–892.
[23] M. Wikström, M.I. Verkhovsky, Mechanism and energetics of proton translocation by the respiratory heme–copper oxidases, Biochim. Biophys. Acta 1767 (2007) 1200–1214.
[24] P.E.M. Siegbahn, M.R.A. Blomberg, Energy diagrams and mechanism for proton pumping in cytochrome *c* oxidase, Biochim. Biophys. Acta 1767 (2007) 1143–1156.
[25] G. Buse, T. Soulimane, M. Dewor, H.E. Meyer, M. Blüggel, Evidence for a copper-coordinated histidine–tyrosine cross-link in the active site of cytochrome oxidase, Protein Sci. 8 (1999) 985–990.
[26] S. Yoshikawa, K. Shinzawa-itoh, R. Nakashima, R. Yaono, E. Yamashita, N. Inoue, M. Yao, M.J. Fei, C.P. Libeu, T. Mizushima, H. Yamaguchi, T. Tomizaki, T. Tsukihara, Redox-coupled crystal structural changes in bovine heart cytochrome *c* oxidase, Science 280 (1998) 1723–1729.
[27] G.T. Babcock, How oxygen is activated and reduced in respiration, Proc. Natl. Acad. Sci. U. S. A. 96 (1999) 12971–12973.
[28] F.G. Wiertz, O.M. Richter, A.V. Cherepanov, F. MacMillan, B. Ludwig, S. de Vries, An oxo-ferryl tryptophan radical catalytic intermediate in cytochrome *c* and quinol oxidases trapped by microsecond freeze-hyperquenching (MHQ), FEBS Lett. 575 (2004) 127–130.
[29] F. MacMillan, K. Budiman, H. Angerer, H. Michel, The role of tryptophan 272 in the *Paracoccus denitrificans* cytochrome *c* oxidase, FEBS Lett. 580 (2006) 1345–1349.
[30] J.E. Morgan, M.I. Verkhovsky, G. Palmer, M. Wikström, Role of the PR intermediate in the reaction of cytochrome *c* oxidase with O_2, Biochemistry 40 (2001) 6882–6892.
[31] E.A. Gorbikova, I. Belevich, M. Wikström, M.I. Verkhovsky, The proton donor for O–O bond scission by cytochrome *c* oxidase, Proc. Natl. Acad. Sci. U. S. A. 105 (2008) 10733–10737.
[32] R.B. Gennis, Coupled proton and electron transfer reactions in cytochrome oxidase, Front. Biosci. 4 (2004) 581–591.
[33] P. Brzezinski, Redox-driven membrane-bound proton pumps, TIBS 29 (2004) 380–387.
[34] A. Kannt, T. Soulimane, G. Buse, A. Becker, E. Bamberg, H. Michel, Electrical current generation and proton pumping catalyzed by the ba3-type cytochrome *c* oxidase from *Thermus thermophilus*, FEBS Lett. 434 (1998) 17–22.
[35] S.A. Siletsky, I. Belevich, A. Jasaitis, A.A. Konstantinov, M. Wikström, T. Soulimane, M.I. Verkhovsky, Time-resolved single-turnover of ba_3 oxidase from *Thermus thermophilus*, Biochim. Biophys. Acta 1767 (2007) 1383–1392.
[36] I.A. Smirnova, D. Zaslavsky, J.A. Fee, R.B. Gennis, P. Brzezinski, Electron and proton transfer in the ba(3) oxidase from Thermus thermophilus, J. Bioenerg. Biomembr. (in press)
[37] R. Mitchell, P. Mitchell, P.R. Rich, The assignment of the 655 nm spectral band of cytochrome oxidase, FEBS Lett. 280 (1991) 321–324.
[38] E.I. Solomon, R.K. Szilagyi, S. DeBeer George, L. Basumallick, Electronic structures of metal sites in proteins and models: contributions to function in blue copper proteins, Chem. Rev. 104 (2004) 419–458.
[39] W. Kaim, B. Schwederski, Biological Chemistry: Inorganic Elements in the Chemistry of Life — An Introduction and Guide, John-Wiley and Sons, 1994, pp. &!#32187–214.
[40] D.A. Proshlyakov, M.A. Pressler, C. DeMaso, J.F. Leykam, D.L. DeWitt, G.T. Babcock, Oxygen activation and reduction in respiration: involvement of redox-active tyrosine 244, Science 290 (2000) 1588–1591.
[41] K.M. McCauley, J.M. Vrtis, J. Dupont, W.A. van der Donk, Insights into the functional role of the tyrosine–histidine linkage in cytochrome *c* oxidase, J. Am. Chem. Soc. 122 (2000) 2403–2404.
[42] Y. Bu, R.I. Cukier, Structural character and energetics of tyrosyl radical formation by electron/proton transfers of a covalently linked histidine–tyrosine: a model for cytochrome *C* oxidase, J. Phys. Chem. B 109 (2005) 22013–22026.
[43] V. Daskalakis, E. Pinakoulaki, S. Stavrakis, C. Varotsis, Probing the environment of cu(b) in heme–copper oxidases, J. Phys. Chem. B 111 (2007) 10502–10509.
[44] P. Hohenberg, W. Kohn, Inhomogeneous electron gas, Phys. Rev. 136 (1964) B864–B871.
[45] W. Kohn, L.J. Sham, Self-consistent equations including exchange and correlation effects, Phys. Rev. 140 (1965) A1133–A1138.
[46] P.E.M. Siegbahn, The performance of hybrid DFT for mechanisms involving transition metal complexes in enzymes, J. Biol. Inorg. Chem. 11 (2006) 695–701.
[47] D. Harris, G. Loew, L. Waskell, Structure and spectra of ferrous dioxygen and reduced ferrous dioxygen model cytochrome *P450*, J. Am. Chem. Soc. 120 (1998) 4308–4318.
[48] P.E.M. Siegbahn, M.R.A. Blomberg, Transition-metal systems in biochemistry studied by high-accuracy quantum chemical methods, Chem. Rev. 100 (2000) 421–437.
[49] A. Ghosh, T. Vangberg, E. Gonzales, P. Taylor, Molecular structures and electron distributions of higher-valent iron and manganese porphyrins. Density functional theory calculations and some preliminary open-shell coupled-cluster results, J. Porphyrins Phthalocyanines 5 (2001) 345–356.
[50] M.P. Johansson, M.R.A. Blomberg, D. Sundholm, M. Wikström, Change in electron and spin density upon electron transfer to haem, Biochim. Biophys. Acta 1553 (2002) 183–187.
[51] M.P. Johansson, D. Sundholm, G. Gerfen, M. Wikström, The spin distribution in low-spin iron porphyrins, J. Am. Chem. Soc. 124 (2002) 11771–11790.
[52] M.P. Johansson, D. Sundholm, Spin and charge distribution in iron porphyrin models: a coupled cluster and density-functional study, J. Chem. Phys. 120 (2004) 3229–3236.
[53] P.E.M. Siegbahn, T. Borowski, Modeling enzymatic reactions involving transition metals, Acc. Chem. Res. 39 (2006) 729–738.
[54] A.D. Becke, Density-functional thermochemistry. III. The role of exact exchange, J. Chem. Phys. 98 (1993) 5648–5652.
[55] C. Lee, W. Yang, R.G. Parr, Development of the Colle–Salvetti correlation-energy formula into a functional of the electron density, Phys. Rev. B 37 (1988) 785–789.
[56] L.A. Curtiss, K. Raghavachari, R.C. Redfern, J.A. Pople, Assessment of Gaussian-3 and density functional theories for a larger experimental test set, J. Chem. Phys. 112 (2000) 7374–7383.
[57] P.E.M. Siegbahn, M.R.A. Blomberg, Density functional theory of biologically relevant metal centers, Annu. Rev. Phys. Chem. 50 (1999) 221–249.
[58] K.P. Jensen, U. Ryde, Theoretical prediction of the Co–C bond strength in cobalamins, J. Phys. Chem. B 107 (2003) 7539–7545.

[59] U. Ryde, K. Nilsson, Quantum chemistry can locally improve protein crystal structures, J. Am. Chem. Soc. 125 (2003) 14232–14233.
[60] K.P. Jensen, B.O. Roos, U. Ryde, Performance of density functionals for first row transition metal systems, J. Chem. Phys. 126 (2007) 014103-1–14.
[61] F. Neese, A critical evaluation of DFT, including time-dependent DFT, applied to bioinorganic chemistry, J. Biol. Inorg. Chem. 11 (2006) 702–711.
[62] A. Ghosh, Transition metal spin state energetics and noninnocent systems: challenges for DFT in the bioinorganic arena, J. Biol. Inorg. Chem. 11 (2006) 712–724.
[63] T. Tsukihara, K. Shimokata, Y. Katayama, H. Shimada, K. Muramoto, H. Aoyoma, M. Mochizuki, K. Shinzawa-Itoh, E. Yamashita, M. Yao, Y. Ishimura, S. Yoshikawa, The low-spin heme of cytochrome *c* oxidase as the driving element of the proton-pumping process, Proc.Natl. Acad. Sci. U. S. A. 100 (2003) 15304–15309.
[64] M.P. Johansson, V.R.I. Kaila, L. Laakkonen, Charge parameterization of the metal centers in cytochrome *c* oxidase, J. Comp. Chem. 29 (2008) 753–767.
[65] A. Schäfer, H. Horn, R. Ahlrichs, Fully optimized contracted Gaussian basis sets for atoms Li to Kr, J. Chem. Phys. 97 (1992) 2571–2577.
[66] A. Schäfer, C. Huber, R. Ahlrichs, Fully optimized contracted Gaussian basis sets of triple zeta valence quality for atoms Li to Kr, J. Chem. Phys. 100 (1994) 5829–5835.
[67] A. Klamt, G. Schüürmann, COSMO: a new approach to dielectric screening in solvents with explicit expressions for the screening energy and its gradient, J. Chem. Soc. Perkin Trans. 2 (1993) 799–805.
[68] E.A. Gorbikova, K. Vuorilehto, M. Wikström, M.I. Verkhovsky, Redox titration of all electron carriers of cytochrome *c* oxidase by Fourier transform infrared spectroscopy, Biochemistry 45 (2006) 5641–5649.
[69] M.W. Palascak, G.C. Shields, Accurate experimental values for the free energies of hydration of H^+, OH^-, and H_3O^+, J. Phys. Chem. A 108 (2004) 3692–3694.
[70] R. Ahlrichs, M. Bär, M. Häser, H. Horn, C. Kölmel, Electronic-structure calculations on workstation computers — the program system Turbomole, Chem. Phys. Lett. 162 (1989) 165–169.
[71] W. Humphrey, A. Dalke, K. Schulten, VMD: visual molecular dynamics, J. Molec. Graphics 14 (1996) 33–38.
[72] L. Laaksonen, A graphics program for the analysis and display of molecular dynamics trajectories, J. Mol. Graphics 10 (1992) 33–34.
[73] D.L. Bergman, L. Laaksonen, A.J. Laaksonen, Visualization of solvation structures in liquid mixtures, J. Mol. Graphics and Modelling 15 (1997) 301–306.
[74] L. Qin, C. Hiser, A. Mulichak, R.M. Garavito, S. Ferguson-Miller, Identification of conserved lipid/detergent-binding sites in a high-resolution structure of the membrane protein cytochrome *c* oxidase, Proc. Natl. Acad. Sci. U. S. A. 103 (2006) 16117–16122.
[75] C. Ostermeier, A. Harrenga, U. Ermler, H. Michel, Structure at 2.7 Å resolution of the *Paracoccus denitrificans* two-subunit cytochrome *c* oxidase complexed with an antibody F_v fragment, Proc. Natl. Acad. Sci. U. S. A. 94 (1997) 10547–10553.
[76] T. Soulimane, G. Buse, G.P. Bourenkov, H.D. Bartunik, R. Huber, M.E. Than, Structure and mechanism of the aberrant *ba*(3)-cytochrome *c* oxidase from *Thermus thermophilus*, EMBO J. 19 (2000) 1766–1776.
[77] C.E. Housecroft, A.G. Sharpe, Inorganic Chemistry 2005, 2nd ed., ISBN 0130-39913-2.
[78] M. Ralle, M.L. Verkhovskaya, J.E. Morgan, M.I. Verkhovsky, M. Wikström, N.J. Blackburn, Coordination of Cu_B in reduced and CO-liganded states of cytochrome bo_3 from *Escherichia coli*. Is chloride ion a cofactor? Biochemistry 38 (1999) 7185–7194.
[79] C. Remenyi, R. Reviakine, M. Kaupp, Density functional study of EPR parameters and spin-density distribution of azurin and other blue copper proteins, J. Phys. Chem. B 111 (2007) 8290–8304.
[80] M.R.A. Blomberg, P.E.M. Siegbahn, M. Wikström, Metal-bridging mechanism for O–O bond cleavage in cytochrome *C* oxidase, Inorg. Chem. 42 (2003) 5231–5243.
[81] H. Lepp, E. Svahn, K. Faxén, P. Brzezinski, Charge transfer in the K proton pathway linked to electron transfer to the catalytic site in cytochrome *c* oxidase, Biochemistry 47 (2008) 4929–4935.
[82] M.I. Verkhovsky, A. Jasaitis, M.L. Verkhovskaya, J.E. Morgan, M. Wikström, Proton translocation by cytochrome *c* oxidase, Nature 400 (1999) 480–483.
[83] D. Bloch, I. Belevich, A. Jasaitis, C. Ribacka, A. Puustinen, M.I. Verkhovsky, M. Wikström, The catalytic cycle of cytochrome *c* oxidase is not the sum of its two halves, Proc. Natl. Acad. Sci. U. S. A. 101 (2004) 529–533.
[84] D. Jancura, V. Berka, M. Antalik, J. Bagelova, R.B. Gennis, G. Palmer, M. Fabian, Spectral and kinetic equivalence of oxidized cytochrome *C* oxidase as isolated and "activated" by reoxidation, J. Biol. Chem. 281 (2006) 30319–30325.